Smart Structures and Systems, *Vol. 18, No. 5 (2016) 931-953*
DOI: http://dx.doi.org/10.12989/sss.2016.18.5.931

Seismic responses of asymmetric steel structures isolated with the TCFP subjected to mathematical near-fault pulse models

H. Tajammolian, F. Khoshnoudian* and V. Bokaeian

Faculty of Civil Engineering, Amirkabir University of Technology (Tehran Polytechnic), Tehran, Iran

(Received January 18, 2016, Revised June 30, 2016, Accepted July 9, 2016)

Abstract. In this paper, the effects of mass eccentricity of superstructure as well as stiffness eccentricity of isolators on the amplification of seismic responses of base-isolated structures are investigated by using mathematical near-fault pulse models. Superstructures with 3, 6 and 9 stories and aspect ratios equal to 1, 2 and 3 are mounted on a reasonable variety of Triple Concave Friction Pendulum (TCFP) bearings considering different period and damping ratio. Three-dimensional linear superstructure mounted on nonlinear isolators are subjected to simplified pulses including fling step and forward directivity while various pulse period (T_p) and Peak Ground Velocity (PGV) amounts as two crucial parameters of these pulses are scrutinized. Maximum isolator displacement and base shear as well as peak superstructure acceleration and drift are selected as the main engineering demand parameters. The results indicate that the torsional intensification of different demand parameters caused by superstructure mass eccentricity is more significant than isolator stiffness eccentricity. The torsion due to mass eccentricity has intensified the base shear of asymmetric 6-story model 2.55 times comparing to symmetric one. In similar circumstances, the isolator displacement and roof acceleration are increased 49 and 116 percent respectively in the presence of mass eccentricity. Furthermore, it is demonstrated that torsional effects of mass eccentricity can force the drift to reach the allowable limit of ASCE 7 standard in the presence of forward directivity pulses.

Keywords: TCFP isolators; near-fault; mathematical pulse model; eccentricity; torsion; steel special moment frames

1. Introduction

The response of structures against harmful effects of earthquake could be controlled by increasing the stiffness, ductility and energy dissipation of the structure. Seismic isolation is a method to reduce the input energy of superstructure by the concept of weak story and significantly decreases structural and non-structural damages under severe ground shakings. Because the structural damage reduction will sustain the operational performance level of the building, base isolating is a favorable way for protection of structures with high importance occupancy through an earthquake.

Despite many base isolation systems have been proposed by investigators, they can be categorized in two main groups: elastomeric and frictional bearing. Single Friction Pendulum (SFP), Double Concave Friction Pendulum (DCFP) and Triple Concave Friction Pendulum (TCFP)

*Corresponding author, Professor, E-mail: khoshnud@aut.ac.ir

http://www.techno-press.org/?journal=sss&subpage=8 ISSN: 1738-1584 (Print), 1738-1991 (Online)

bearings are among the latter group. The section of a TCFP isolator can be seen in Fig. 1(a). It is made up of four concave plates that are separated by an articulated slider in the middle of them. The bottom sliding edges are called 1 and 2 while the top plates denotes by 3 and 4. The radius of each sliding plate denotes R_i and its displacement capacity stands for d_i. The sliding plates are covered by a non-metallic material with friction coefficient of μ_1 to μ_4. By thoroughly adjustment of plates' radii and friction coefficient a 5-regime backbone μ_1 curve μ_4 can be obtained that is illustrated in Fig. 1(b) (Loghman and Khoshnoudian 2015).

The main advantage of TCFP bearing in comparison with SFP and DCFP ones, that have bilinear and tri-linear behaviors respectively, is the hardening regimes at the end of its backbone curve. As an example, the stiffness at the end of 3rd regime of the motion (K_{eff3}) as well as 5th regime (K_{eff5}) is presented in Fig. 1(b). Obviously K_{eff5} is greater than K_{eff3}, so TCFP bearing is expected to experience smaller displacement comparing with SFP and DCFP isolators under strong ground excitations. This fact is expressed by Tajammolian *et al.* (2014).

Many investigators have been made to present an adaptive model for predicting the TCFP bearings seismic behavior. Fenz and Constantinou (2008a,b) have introduced the first model. This model consists of three SFP elements connected in series for idealizing the adaptive behavior of the TCFP isolator. In current research, we have employed this model for estimating seismic performance of TCFP base-isolated structures. Therefore, extensive explanation will be presented in chapter 3. A new model for predicting the responses of the TCFP isolated structures subjected to bi-directional ground motions was proposed by Becker and Mahin (2012, 2013). Dao, Ryan *et al*. (2013) have modified the series model introduced by Fenz and Constantinou with adding a circular gap element which enables it to simulate three-dimensional behavior of structures isolated with TCFP bearings. They have made the experimental tests to verify their new model and have implemented the TCFP isolator element in OpenSees software. Sarlis and Constantionu (2013) have improved the formulations of force-displacement equations for TCFP bearing in a way that can predict its real behavior in uplift conditions.

Morgan and Mahin (2010, 2011) have studied the performance of base-isolated structures mounted on TCFP bearings in different damage states subjecting to earthquakes with various intensity levels. The effect of vertical component of near-fault earthquakes was investigated by Loghman and Khoshnoudian (2015). They revealed that neglecting the effect of vertical component can cause notable errors in predicting the base shear of low-rise structures. Tajammolian, Khoshnoudian *et al*. (2014) scrutinized the responses of a Single Degree of Freedom (SDF) superstructure on TCFP bearings subjected to simplified forward directivity and fling step pulse models.

Jangid and Kelly (2001) studied the responses of superstructures rested on different elastomeric isolators subjected to six pairs of horizontal components of near-fault records. Jangid (2005) notified that the optimum friction coefficient is found to be in the range of 0.05 to 0.15 in SFP isolators for controlling the responses of a structure subjected to near-fault ground motions. Variable Friction Pendulum System (VFPS) that improved the performance of SFP isolator in near-fault motions was proposed by Panchal and Jangid (2008). Dicleli (2007) and Dicleli and Buddaram (2007) have investigated the utilization of isolators with bilinear backbone curve in protection of bridges against near-field earthquakes. The effects of earthquakes on seismic responses of isolated structures mounted on SFP, DCFP and TCFP bearings were studied by researchers regardless to torsion (Loghman and Khoshnoudian 2015, Bagheri and Khoshnoudian 2014, Khoshnoudian and Rabiei 2010, Rabiei and Khoshnoudian 2011, 2013, Khoshnoudian and Rezai Haghdoost 2009).

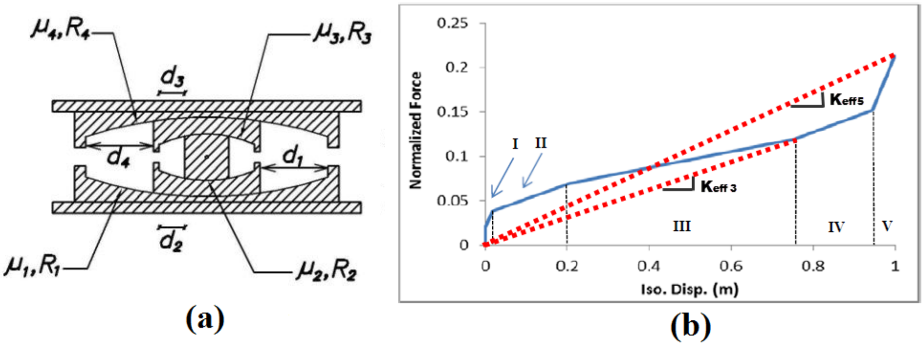

Fig. 1 (a)TCFP isolator section and (b)backbone curve of a TCFP (Loghman *et al.* 2015)

Two types of eccentricities should be taken into account in the torsionally coupled base-isolated structures: mass eccentricity in superstructure and stiffness eccentricity in isolators (Kilar and Koren 2009). Zayas, Low *et al.* (1987, 1989) have demonstrated that SFP isolators are capable of controlling the torsional responses of one story structures with mass eccentricity. Almazan and De la Llera (2003) evaluated the effects of accidental eccentricity caused by overturning in the seismic response of symmetric structures supported on SFP bearings. They also conducted some experimental tests and concluded that the mass eccentricity can increase the isolator displacement up to 6% in 3-story isolated structure (De la Llera and Almazan 2003).

Different distributions of Center of Mass (CM) in superstructure and Center of Stiffness (CS) of LRB isolators were examined by Kilar and Koren (2009). They revealed that while CS is moved into the mirror position of CM (i.e., CS=-CM) the isolator displacement may be amplified up to 1.4 comparing with the symmetric case (CS=CM) under bidirectional far-field earthquakes.

Tena-Colunga and Gomez-Soberon (2002) investigated the torsional response of base-isolated structures with mass eccentricity. Tena-Colunga and Escamilla-Cruz (2007) scrutinized the torsional effects in base-isolated structures with elastomeric bearing when eccentricity occurs both in the superstructure and isolator. They finalized that the eccentricity related to mass in the superstructure leads to higher torsional amplifications in the bearings displacements than stiffness eccentricity of the isolators. The effect of eccentricities in isolators was examined by Tena-Colunga and Zambrana-Rojas (2006) using a bilinear isolation system subjected to unidirectional and bidirectional actions of selected earthquakes.

Khoshnoudian and Imani Azad (2011) considered the mass eccentricity as well as stiffness eccentricity of isolators in their investigation. They noted that in a bilinear isolation system, the effects of bidirectional near-fault ground motions would magnify the torsional intensification comparing with unidirectional records. Khoshnoudian and Motamedi (2013) revealed that ignoring vertical component of earthquake in steel structures mounted on elastomeric isolators results unacceptable estimation in superstructure beam shear and column axial forces. Finite element analysis of various eccentricities in superstructure and nonlinear elastomeric isolating system is scrutinized by Khoshnoudian and Azizi (2007). Fallahian, Khosnoudian *et al.* (2015) investigated the responses of torsionally coupled base-isolated structures rested on TCFP bearings subjected to bidirectional near field ground motions. They have compared the results of TCFP base-isolated structures with those supported on SFP or DCFP isolators as well. Tajammolian, Khoshnoudian *et al.* (2016) scrutinized the effect of mass asymmetry on the responses of structures mounted on TCFP when they are subjected to three components of near-fault earthquake records. De la Llera and Chopra (1994), Jangid and Datta (1995), Ryan and Chopra (2006), Picazo, Lopez *et al*. (2015) and Siringurino and Fujino (2015) have investigated the torsional responses of base-isolated structures under different ground motions, as well.

Although many investigations have been conducted in order to study the torsional behavior of base-isolated structures with elastomeric or SFP bearings, the seismic behavior of structures isolated with TCFP with mass or stiffness eccentricity have not been addressed yet. As discussed earlier, TCFP have a 5-regimes backbone curve with hardening behavior in phases 4 and 5 of motion. Therefore, this hardening is expected to control the responses amplification due to torsion in TCFP base isolated structures, better than SFP and DCFP ones. In this regards, different kinds of eccentricities, namely mass in superstructure (E_S) and stiffness in bearing (E_B) as well as their simultaneous occurrences ($E_{S\&B}$) are considered in this study. Additionally, mathematical pulse models of forward directivity and fling step ground motions are selected in order to investigate the influence of pulse period (T_p) as well as Peak Ground Velocity (PGV) of earthquake. These two parameters are the key characteristics of near-fault motions which will be discussed in chapter 2. This study focuses on the torsional effects of near-fault excitations on the engineering demand responses, such as isolation displacement, base shear, roof acceleration and interstory drift of superstructures mounted on TCFP isolators. TCFP bearings with a reasonable range of effective periods and damping ratios are considered, while various slenderness (Height/Width) and aspect (Length/Width) ratios of superstructure are assumed.

2. Mathematical pulse models

Near-fault seismic excitations have some prominent characteristics that make them different from far-fault ground motions. High-frequency component in acceleration records as well as long-period velocity pulses are two remarkable specifications of these ground motions (Masaeli, Khoshnoudian *et al*. 2014). Baker (2007) has used wavelet analysis to extract the velocity pulse from a near-fault ground motion. He has decomposed a record into two main parts: extracted pulse and high-frequency motion. This study used the size of extracted pulse to categorize near-fault records as pulse-like or non-pulselike. The pulse-like ground motions can force different structures into extreme demands that are not predicted by typical measures such as response spectra (Bertero, Mahin *et al*. 1978, Hall, Heaton *et al.* 1995, Akkar, Yazgan *et al*. 2005).

Long-period velocity pulses in near-fault excitations may have different seismological sources. In forward directivity pulses, the ground motion is noticeably affected by the orientation of rupture propagation; while in fling step ones static displacement of ground surface is the main reason of excitation. Among different types of long-period pulses, it has been proven that forward directivity pulses with large amplitude have the most destructive effects on seismic performance of the structures (Baker 2007). As a result, many authors have made attempts to analysis and evaluate the seismic performance of different structures under forward directivity pulses (Zhang and Tang 2009, Khoshnoudian and Ahmadi 2013, Galal and Naeim 2008).

In this investigation, the input excitations are selected accurately to enable the parametric study of pulse period as well as its PGV. For this reason, using simplified sinusoidal pulse for both fling step and forward directivity effects is employed. For the first time, Sasani and Bertero (2000) and

Agrrawal and He (2002) proposed the utilization of these pulses instead of near-fault original excitations and it was later implemented by Kalkan and Kunnath (2006) as well as Khoshnoudian and Ahmadi (2013). Obviously it is not expected that synthetic pulses can completely predict all characteristics of the main records, especially for complicated frequency-content ground motions. However, Sasani and Bertero (2000), and Krawinkler and Alavi (1998) have stated that simple pulses can be used to capture the notable response properties of structures subjected to near-field excitations. Alavi and Krawinkler (2004) analyzed some steel moment frames under both actual near-fault ground motions and the simplified mathematical pulses. They revealed that the most important features in frame responses can be adequately captured by simplified pulses. Kalkan and Kunnath (2006) used sine pulses and revealed that these pulse models can estimate the effects of higher modes of structure with minimum error.

Simplified pulses that are used in this study are sinusoidal functions as presented in Fig. 2. In the fling step pulse which is shown in Fig. 2(a), a static offset can be seen at the end of the displacement time history. On the other hand, forward directivity pulse has no residual motion at the end of its displacement phase (Fig. 2(b)). It has been affirmed that forward directivity pulses have duration in the range of 1.5 to 2.5 times the duration of fling step ones (Khoshnoudian and Ahmadi 2013). According to Fig. 2, the duration of the forward directivity pulse is assumed 1.5 times the duration of the fling step one. Note that Kalkan and Kunnath (2006) and Khoshnoudian and Ahmadi (2013) assumed this value in their investigations too. To fulfill the objective of performing a deep sensitivity analysis, pulse amplitude (T_p) is selected in the range of 1 to 10 second. In addition, the pulses are scaled such that their velocity time history exhibit its peak value (PGV) equal to 40, 80, 120, 160 and 200 cm/s.

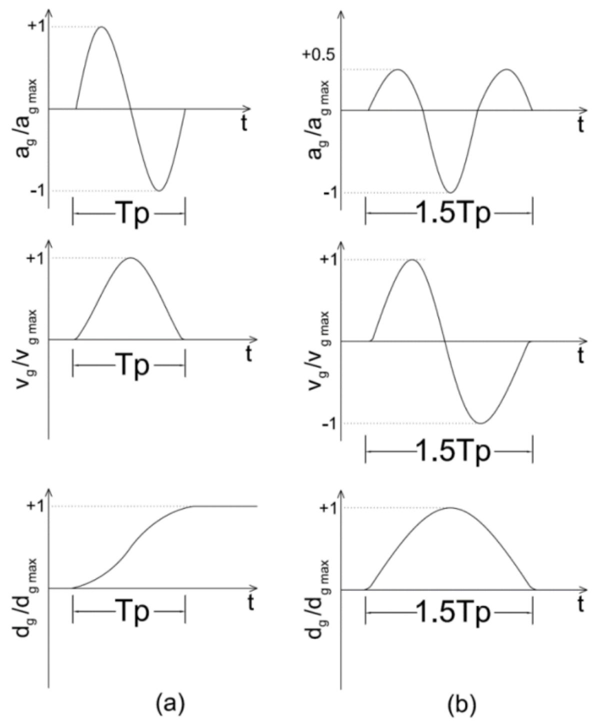

Fig. 2 Simplified near-fault pulse (a) Fling step and (b) Forward directivity (Sasani and Bertero 2000)

3. Mathematical modeling of TCFP

The behaviour of TCFP bearing is more complicated than the other concave friction pendulum isolators because it has more sliding surfaces (Fig. 1). Its behaviour has a backbone curve with five different phases of motions. In the regimes I to III, the isolator displacement is in a softening manner while the curve slope changes in phases IV and V and becomes stiffer. The fully adaptive movement of the isolator will happen when the friction coefficients of sliding plates is $\mu_2=\mu_3<\mu_1<\mu_4$. Fenz and Constantinou (2008a) proposed a method to simulate multi-spherical sliding isolators' behavior. In their method three SFP elements can be used in order to idealize a TCFP model. It should be noted that despite the fact that a TCFP is made up of four sliding surfaces, the two inner plates (surfaces 2 and 3 in Fig. 1(a)), commonly have similar radii and friction coefficients; therefore they can be modeled by one SFP element. In addition to SFP elements, some gap elements are used in this model to simulate the hardening behavior of regimes IV and V. The series model was developed in SAP2000 software (Fig. 3).

The horizontal force F_i for each SFP element is given in Eqs. (1) to (3) that can be obtained from their equations of motions

$$F_i = \frac{W}{R_{effi}} u_i + \mu_i W \ Z_i + F_{ri} \tag{1}$$

$$\frac{dZ_i}{dt} = \frac{1}{u_{yi}} \left\{ A_i - \left|Z_i\right|^{\eta_i} \left[\gamma_i \ sign(\dot{u}_i Z_i) + \beta_i \right] \right\} \dot{u}_i \tag{2}$$

$$F_{ri} = k_{ri} \left(\left|u_i\right| - d_i \right) sign\left(u_i\right) H\left(\left|u_i\right| - d_i\right) \tag{3}$$

Where:

u_i and $\dot{u}_i$: the bearing displacement and velocity,

W: the weight of structure,

R_{effi}: the effective radius of curvature of the sliding surface,

μ_i : the coefficient of friction,

Z_i: a dimensionless hysteretic variable,

F_{ri}: the contact effect with restrainers,

u_{yi}: the yield displacement

$A_i, \eta_i, \gamma_i, \beta_i$: dimensionless quantities that control the shape of the hysteresis loop,

k_{ri} : the stiffness after contacting the displacement restrainers which is assigned a large value,

H: Heaviside function.

The restrainer of each sliding plate is assumed to be nearly rigid. This assumption is considered in most investigations related to the modeling of TCFP bearings, e.g., Fenz and Constantinou (2008a), Morgan and Mahin (2011) and Becker and Mahin (2012). The real stiffness of the restrainer part should be modified according to experimental tests. In this research, this value was selected according to Fenz and Constantinou (2008a) assumptions. In addition, the properties of the TCFP isolator, i.e., R_1 to R_4 and μ_1 to μ_4, should be modified for utilizing in the three-element series model. The formulas for this modification can be found in Fenz and Constantinou investigation (2008b). The effective damping (ξ_{eff}) and period (T_{eff}) of the isolators are commonly used in seismic codes as their design parameters. These two parameters can be computed according to Eqs. (4) and (5)

$$T_{eff} = 2\pi\sqrt{\frac{W}{K_{eff}\ g}} \tag{4}$$

$$\xi_{eff} = \frac{1}{2\pi}\left[\frac{E_{loop}}{K_{eff}\ D^2}\right] \tag{5}$$

In these equations K_{eff} indicates the effective linear stiffness of the isolator and E_{loop} denotes the energy dissipated in each cycle of the hysteresis loop. E_{loop} and K_{eff} can be calculated according to the procedure described by Becker and Mahin (2012). D is the target displacement of the isolator at the end of sliding regime IV that can be computed by the formulas introduced in ASCE 7-2010. The displacement capacity of the isolators with T_{eff} equal to 3, 4 and 5s used in this research is assumed as 1.0 m. It should be noted that the Maximum Considered Earthquake (MCE) hazard level is assumed for the design of TCFP isolators. Different ranges of possible friction coefficient are reported in literature. Morgan and Mahin (2010) have identified 0.01 to 0.02, 0.05 to 0.08 and 0.1 to 0.2 as low, medium and high friction ranges in the same order. This definition is used in the current investigation, too.

4. Design of superstructure

In order to investigate the effects of torsion on base-isolated structures, five superstructures are designed (Table 1). These five superstructures are selected to create a reasonable range of superstructure specifications, i.e. slenderness and aspect ratios. As seen in Table 1, the aspect ratio of superstructures that is the indicator of its plan length to width ratio (a/b) is equal to 1, 2 and 3. Both square and rectangular plans are considered. The slenderness ratio, i.e. structure height to plan width (H/b), suggests 0.67, 1.33 and 2. The behavior of an isolated structure is dominated by the behavior of isolation level and not as much by the details of the model of the superstructure (Almazan and De la Llera 2003), for this reason the superstructure is linearly modeled. Note that in cases that the pounding between slider and restrainer of the isolator occurs, some parts of the superstructure may experience nonlinear behavior. However, this pounding is avoided in the most of the designed bearings of this investigation; therefore, using the linear model for superstructure seems acceptable. Our reference model is the superstructure No. 2 in Table 1, which is illustrated in Fig. 4. This structure has three bays in length and in width and has 6 stories. The length of each bay is 5 m while the height of each story is assumed 3.33 m; therefore, the total height of the reference superstructure is 20 m. Dead and Live loads are selected as 8 and 4 kN/m^2 according to ASCE 7-10 respectively. The seismic load is calculated by the Equivalent Lateral Force (ELF) method. The seismic analysis of the superstructure with more than 20m height, i.e., structure No. 3, is checked using the Response Spectrum Procedure of ASCE 7-10 document, as well (ASCE 7, 2010). Note that superstructures No. 4 and 5 have six and nine bays in length respectively.

The superstructures consist of steel special moment frames which are designed according to the LRFD method of AISC Specifications for Structural Steel Buildings (AISC 360, 2010) and the design was verified with minimum requirements of AISC Seismic Provisions for Structural Steel Buildings (AISC 341, 2010). The design yield stress of steel material is 240 MPa and its elasticity modulus is $2*10^5$ MPa. Box-type square sections are assumed for columns and standard W-shaped profiles are used as beams. The proportioned sections of superstructures are illustrated in Table 1.

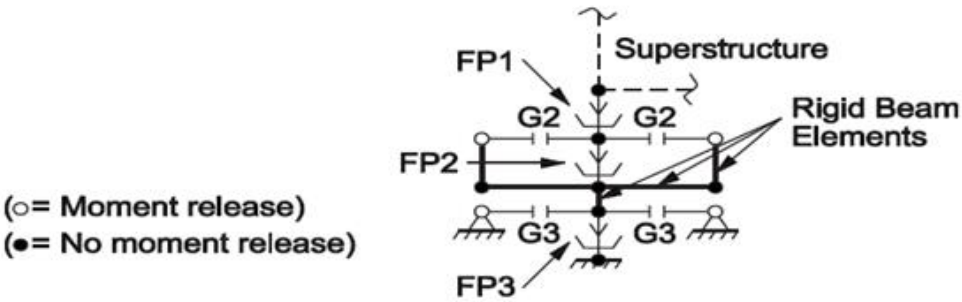

Fig. 3 Series model of TCFP in SAP2000 (Fenz and Constantinou 2008b)

Table 1 Properties of superstructures and designed sections

No.	a (m)	b (m)	H (m)	β=H/b	γ=a/b	Story	Beam Section	Column Section
1	15	15	10	0.67	1	1	W 12×50	B 250×15
						2	W 12×35	B 200×15
						3	W 12×26	B 200×15
2	15	15	20	1.33	1	1	W 12×96	B 350×20
						2	W 12×96	B 300×15
						3	W 12×65	B 300×15
						4	W 12×65	B 250×15
						5	W 12×50	B 250×15
						6	W 12×26	B 200×15
3	15	15	30	2	1	1	W 12×120	B 400×20
						2	W 12×120	B 350×20
						3	W 12×96	B 350×20
						4	W 12×96	B 350×20
						5	W 12×96	B 300×15
						6	W 12×65	B 300×15
						7	W 12×50	B 250×15
						8	W 12×35	B 250×15
						9	W 12×26	B 200×15
4	30	15	20	1.33	2	1-6	same as No. 2	same as No. 2
5	45	15	20	1.33	3	1-6	same as No. 2	same as No. 2

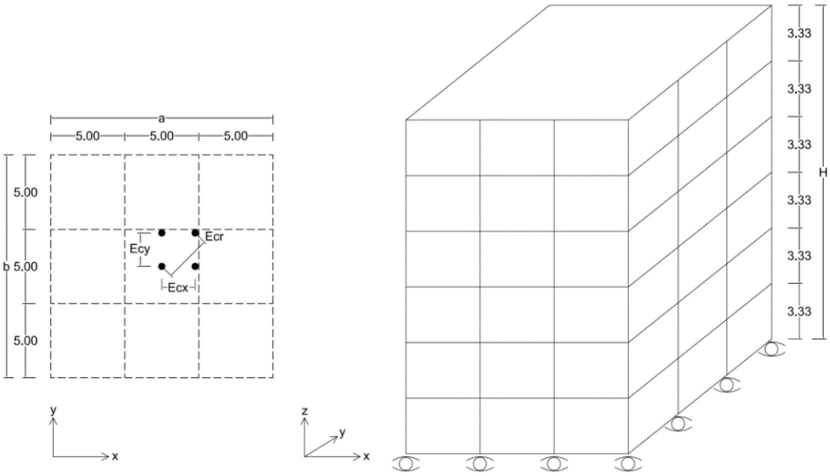

Fig. 4 Plan and view of reference structure

5. Effects of key parameters of near-field earthquakes

To study the influence of near-fault earthquakes on the responses of structures isolated with TCFP bearings, maximum isolator displacement and base shear of the structures are examined. In addition, maximum roof acceleration of superstructure and the peak interstory drift are scrutinized. Note that the drift of base-isolated structure is small; therefore it is only discussed in section 6.2. Three-dimensional structure in Fig. 4 is subjected to mathematical near-field pulse models in y direction and the resultant vector of responses for x and y directions is obtained.

5.1 PGV Effect

Fig. 5 depicts the maximum base shear of structure, isolator displacement and roof acceleration for structures with slenderness ratio (β) of 0.67, 1.33 and 2. All the models have isolators with T_{eff}=5s and ξ_{eff}=15% subjected to fling step and forward directivity pulses with T_p=2s and various PGV values.

The Fig. 5 reveals that the PGV growth causes to increase all the essential responses. However, the rate of this increase is not the same for all the graphs. The isolator has reached its maximum displacement capacity (1 m) in high amounts of PGV, namely 200 cm/s for fling step and more than 120 cm/s for forward directivity pulses; then because of isolator pounding with its restrainer, the model temporarily behaves like a fixed-base structure. As a result, the base shear and roof acceleration are soared significantly. In 6-story model with β=1.33, base shear is reached to 0.23W and 0.53W under fling step and forward directivity pulses respectively, while W stands for the total weight of superstructure. Similarly, the maximum roof acceleration subjected to two simplified pulse models are 0.37g and 1.43g. The pounding between isolator slider and restrainer is discussed extensively later.

As is illustrated in Fig. 5, the forward directivity pulses are more destructive than fling step ones. It is rational since the duration of forward directivity pulses is 1.5 times of the fling step; thus, the superstructure experiences the forward directivity pulses for a longer period of time. Because the PGV is calculated as the integration of acceleration time history from 0 to $0.5T_p$ (Fig. 2) for fling step and also forward directivity pulses with the same PGV, the maximum acceleration (PGA) of forward directivity pulse is 2 times the fling step one's. Khoshnoudian and Ahmadi (2013) also demonstrated that the effects of forward directivity pulses are more severe compared with fling step ones in conventional structures considering soil-structure interaction. The results are conformity with Tajammolian, Khoshnoudian *et al.* (2014) investigation while the two-dimensional SDF models supported on SFP, DCFP and TCFP bearings were studied.

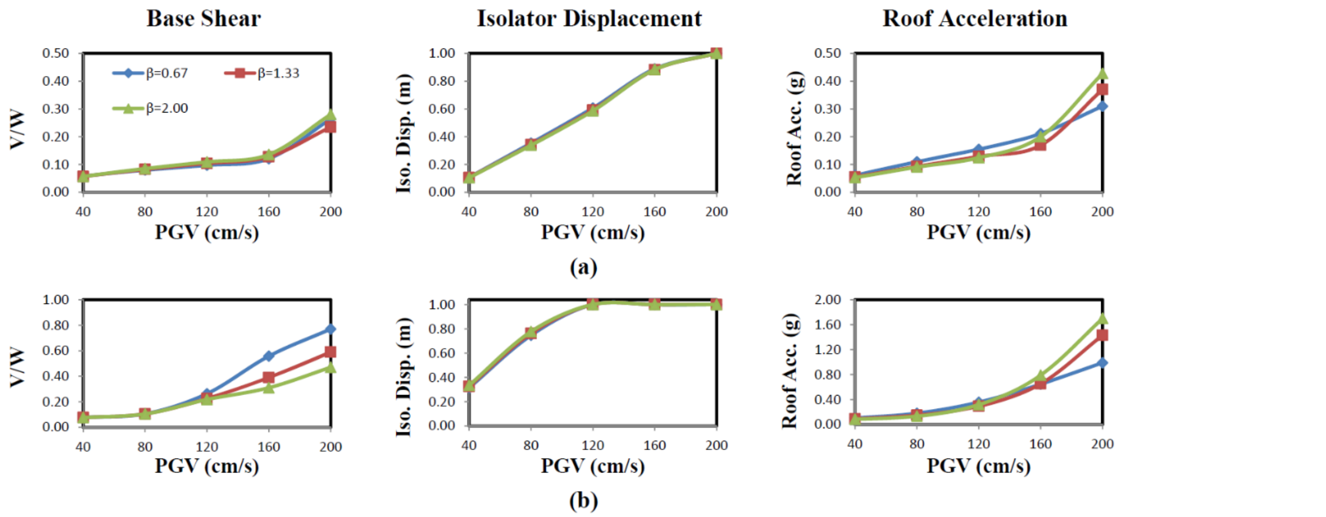

Fig. 5 Responses of structures with different slenderness ratio (β) subjected to simplified pulses assuming γ=1 and T_p=2s (a) Fling step and (b) Forward directivity

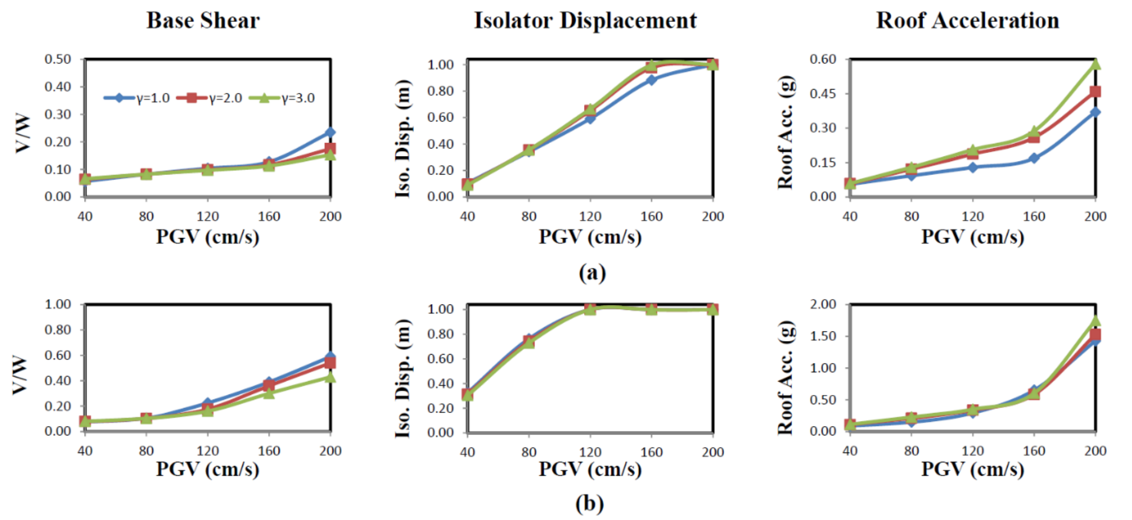

Fig. 6 Responses of structures with different aspect ratio (γ) subjected to simplified pulses assuming β=1.33 and T_p=2s (a) Fling step and (b) Forward directivity

The peak quantities of different responses of structures with various aspect ratio (γ) under near-fault pulses assuming T_p=2 are presented in Fig. 6. Similar to the Fig. 5, TCFP isolators with T_{eff}=5s and ξ_{eff} =15% are employed. It is demonstrated that increasing the PGV raises the responses. In a superstructure with γ=3, the maximum base shear, isolator displacement and roof acceleration under forward directivity pulse is 0.43W, 1m and 1.75g in the same order. It is noted that acceleration values more than g are reported in base-isolated structures by other investigators e.g., Morgan and Mahin (2010) too. The superiority of forward directivity results comparing with fling step pulses is similar to Fig. 5.

The results of Figs. 5 and 6 confirm that the superstructure has smaller effect on the base shear and isolator displacement. However, it has affected the roof acceleration for high amounts of PGV. For instance, increasing the β from 0.67 to 2 in Fig. 5 grows the acceleration form 0.99g to 1.7g in a superstructure subjected to forward directivity pulse with PGV=200 cm/s. Another important point is that increasing the PGV decreases the rate of displacement intensification. Thereby in the both pulses the maximum displacement is limited to 1m at the end of the graph. Because in regimes IV and V of isolator behavior the stiffness is more than regimes I to III, the displacement of pulses with high PGV is controlled efficiently by TCFP hardening phases. Note that these hardening phases are advantages of TCFP in comparison with SFP or DCFP.

The hysteresis curves of an isolator with T_{eff}=5s and ξ_{eff} =15% corresponding to the reference model (Fig. 4) subjected to two different near-fault pulses assuming T_p=2s are drawn in Fig. 7. As discussed earlier, the increase of PGV escalates the base shear and displacement. Consequently, the isolator reaches its displacement capacity i.e., 1 m under fling step pulse with PGV=200 and in forward directivity pulses that have more than 120 cm/s velocities. After this point, the pounding between slider and restrainer forces the base shear to soar substantially.

Two significant points should be taken into consideration in Fig. 7. Firstly, the stiffness of gap element in Fenz and Constantinou (2008b) series model is not infinite; hence, after the isolator pounding with restrainer the displacement grows beyond the isolator capacity e.g., nearly 1.5 m in Fig. 7(b). It should be noted that in all the models in which the maximum isolator displacement grows beyond the isolator capacity, the increase is ignored and the displacement assumed equal to 1m. Secondly, some isolators subjected to high velocity pulses transiently experience uplift, but it does not ended to overturning of whole structure. This uplift can be seen as some fluctuations in force-displacement curves of Fig. 7(b).

5.2 T_p Effect

The effect of forward directivity and fling step pulses with various T_p, from 1 to 10s and a constant PGV value equal to 120 cm/s are scrutinized. The variation of isolated structure responses assuming β=1.33, γ=1, T_{eff}=5s and ξ_{eff} =15% versus the change of pulse period is presented in Fig. 8 as an example. As discussed earlier the superstructure properties have negligible effects on the responses; thus, only the results of a reference superstructure are explained in this chapter.

According to Fig. 8, increasing the T_p from 1s to 4s raises all the responses especially under forward directivity pulses; whereas, the responses decrease when the T_p grows from 4s to 10s. The maximum values of base shear, displacement and roof acceleration are 0.63W, 1m and 1.39g respectively under forward directivity pulse with T_p=4s. It can be well justified by the fact that increasing the T_p to amounts close to the effective isolator period (T_{eff} =5s), intensifies the responses.

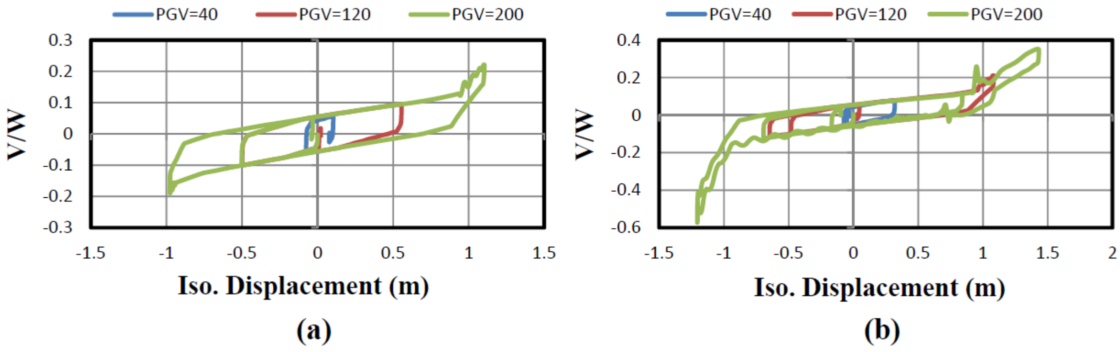

Fig. 7 Force-displacemet of isolator with T_{eff}=5s, ξ_{ef} =15% under T_p=2s pulse (a) Fling step and (b) Forward directivity

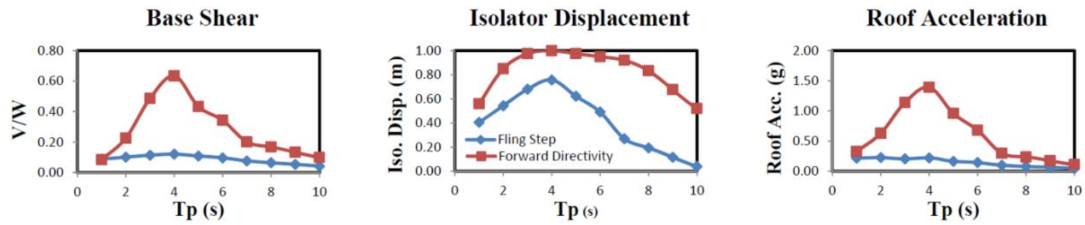

Fig. 8 Responses of structure assuming β=1.33, γ=1 under simplified pulses with PGV=120 cm/s

Kalkan and Kunnath (2006), Ghahari and Khaloo (2013) and Khoshnoudian and Ahmadi (2013) demonstrated this fact for fixed-base structures. They have revealed that structures subjected to simplified pulses with the period range of $0.5T_1$ to $1.5T_1$ while T_1 stands for the fundamental natural period of structure, exhibit more destructive responses than other periods. Note that in this paper, the effective damping of utilized isolators is more than 10%, accordingly the amplification effects are reduced to some extent.

Another important point is that, the PGA of the pulses with the longer T_p is less than pulses with shorter period because they have equal PGV values. For instance, the PGA of a forward directivity pulse with T_p=1s and PGV=120 cm/s is 0.768g while it is less than 0.075g for the similar pulse assuming T_p=10s. Consequently, it is rational that increasing the T_p decreases the responses. Finally, the interaction of these two events makes the isolated structures under near-field earthquakes with the pulse period range of 2s to 6s to experience more destructive responses.

The forward directivity responses are greater than fling step ones in Fig. 8. Considering near-field earthquakes with T_p=4s, isolator displacement due to forward directivity is 32 percent more than the fling step pulse. This increase was reported between 50 to 80 percent for SDF structures and two-dimensional analysis in the previous investigation too (Tajammolian, Khoshnoudian *et al*. 2014).

According to the Figs. 5, 6 and 8 the effect of PGV for the intensification of responses is more than T_p. This conclusion is in accordance with previous study on SFP, DCFP and TCFP isolators (Tajammolian, Khoshnoudian *et al*. 2014).

6. Mass and stiffness eccentricity

To highlight the role of superstructure mass eccentricity as well as isolator stiffness eccentricity in amplification of the responses of base-isolated structure, three categories of eccentricity are considered. All three kinds of eccentricity can be seen in Fig. 4.

1- Longitudinal eccentricity (e_{cx}) with the values of 5, 10, 15 and 20% of plan length (a).
2- Transversal eccentricity (e_{cy}) with the values of 5, 10, 15 and 20% of plan width (b).
3- Diagonal eccentricity (e_{cr}) with the values of 5, 10 and 15% of plan diagonal (r= $(a^2+b^2)^{1/2}$).

To evaluate the influence of each kind of eccentricity, eccentricity in mass of the superstructure (E_S) and stiffness of isolators (E_B) as well as their simultaneous occurrences ($E_{s\&B}$) are studied. The peak amounts of base shear, isolator displacement and roof acceleration are selected as the main engineering demand parameters in a base-isolated structure. To facilitate the study, the “Amp. Factor” is defined as the ratio between response in the asymmetric model and the similar response in the symmetric structure according to Eq. (6).

$$Amp.\ Factor = \frac{RESPONSE\ (Assymetric\ Model)}{RESPONSE\ (Symmetric\ Model)} \tag{6}$$

All the structures presented in Table 1 are analyzed subjected to forward directivity and fling step pulses with T_p=1s-10s and PGV=40-200 cm/s in symmetric and asymmetric cases. Remember that the models are subjected to mathematical near-field pulses in transverse (y) direction. To better illustrate the maximum effect of eccentricity, peak value of calculated “Amp. Factor” among all results is selected for each asymmetric model.

Note that the structure is subjected to uni-directional simplified pulse excitation. According to previous studies, a bi-directional excitation will increase the "Amp. Factor" of the displacement responses not more that 15% (Khoshnoudian and Imani Azad 2011).

6.1 Eccentricity of 6-story model

In order to clarify the influence of each kind of eccentricity, namely E_S, E_B and $E_{S\&B}$, the results of a 6-story model with γ=1 mounted on TCFP isolator with T_{eff}=5s and ξ_{eff} =15% is investigated in this chapter. Note that similar trends were obtained for other superstructures and different isolators too.

The maximum Amp. Factor for different responses in a structure with mass eccentricity (E_S) is presented in Fig. 9. It is clear from the Fig. that the transversal eccentricity (e_{cy}) yields for the intensification of base shear more than other eccentricities i.e., longitudinal and diagonal. The base shear graph reaches its maximum in e_{cy}=20% of plan width, which is 1.66 and 2.55 under fling step and forward directivity pulses respectively. The main reason can be addressed to the horizontal force of friction isolators that is dependent to their vertical load. It means that more weight on a frictional bearing will cause greater lateral force. The transversal mass eccentricity along the direction of applied pulses i.e., y direction produces a rocking motion in the structure. This rocking motion increases the weight on some isolators whereas reduces the weight on the others; consequently, greater base shear in the structure happens.

The amplification of isolator displacement and roof acceleration is significantly related to longitudinal eccentricity (e_{cx}). The graphs of isolator displacement in fling step and roof acceleration in forward directivity pulse experience an Amp. Factor up to 1.30 and 1.29 respectively in e_{cx}=20% of plan length. It can be justified that because the distance of center of mass and center of rigidity of isolators is larger in plans with longitudinal eccentricity, the displacement as well as acceleration will be more affected by the torsion in comparison with the plans with transversal or diagonal eccentricities. It should be remembered that the pulses are applied in y direction. Note that in all the graphs, the diagonal eccentricity Amp. Factor is among the results of longitudinal and transversal ones which is rational. In addition, in most responses forward directivity pulses have greater Amp. Factor than fling step ones.

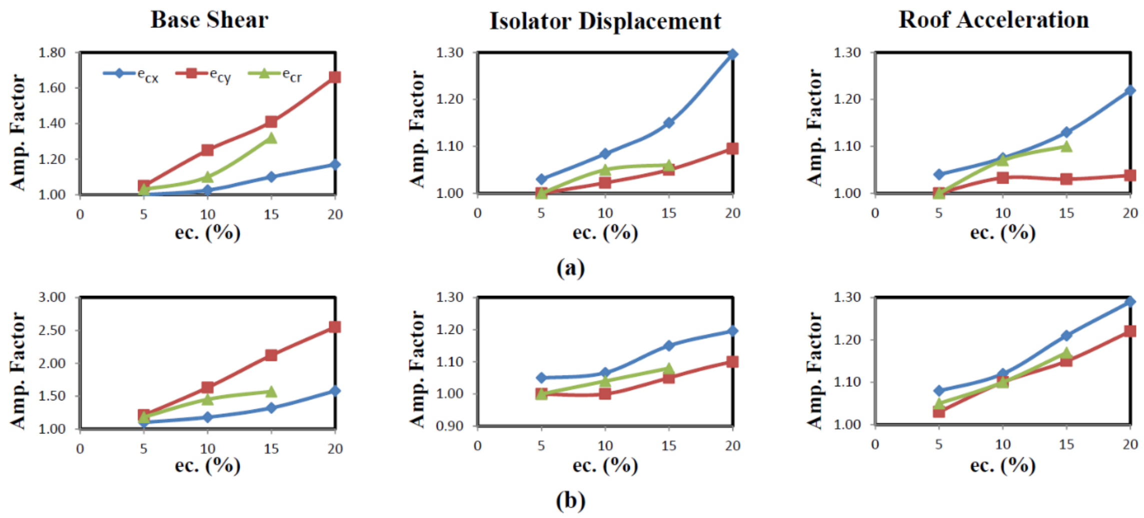

Fig. 9 Maximum Amp. Factor resulted from E_S in structure with β=1.33, γ=1 under simplified pulses having T_p=1-10s , PGV=40-200 cm/s (a) Fling step and (b) Forward directivity

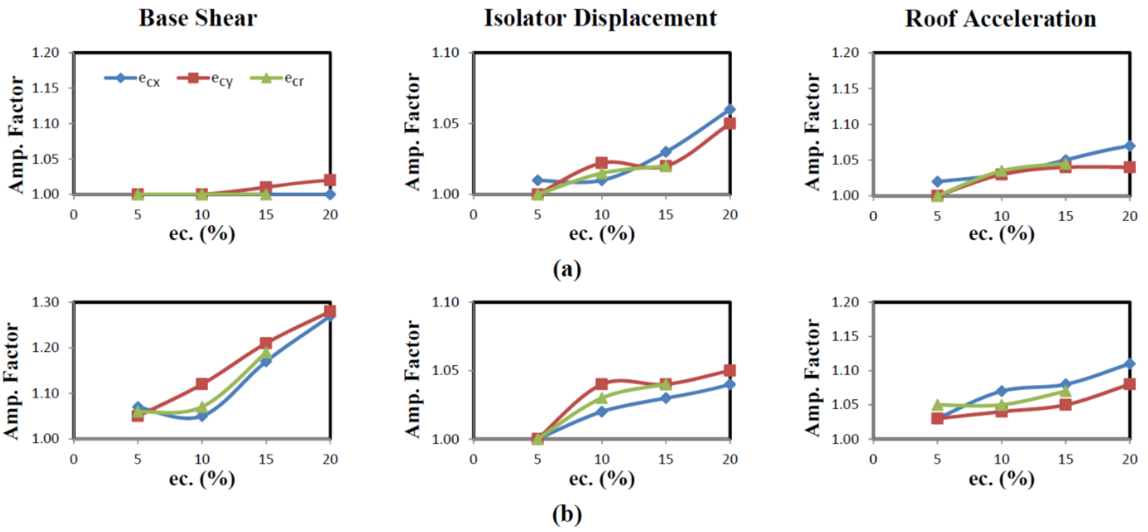

Fig. 10 Maximum Amp. Factor resulted from E_B in structure with β=1.33, γ=1 under simplified pulses having T_p=1-10s , PGV=40-200 cm/s (a) Fling step and (b) Forward directivity

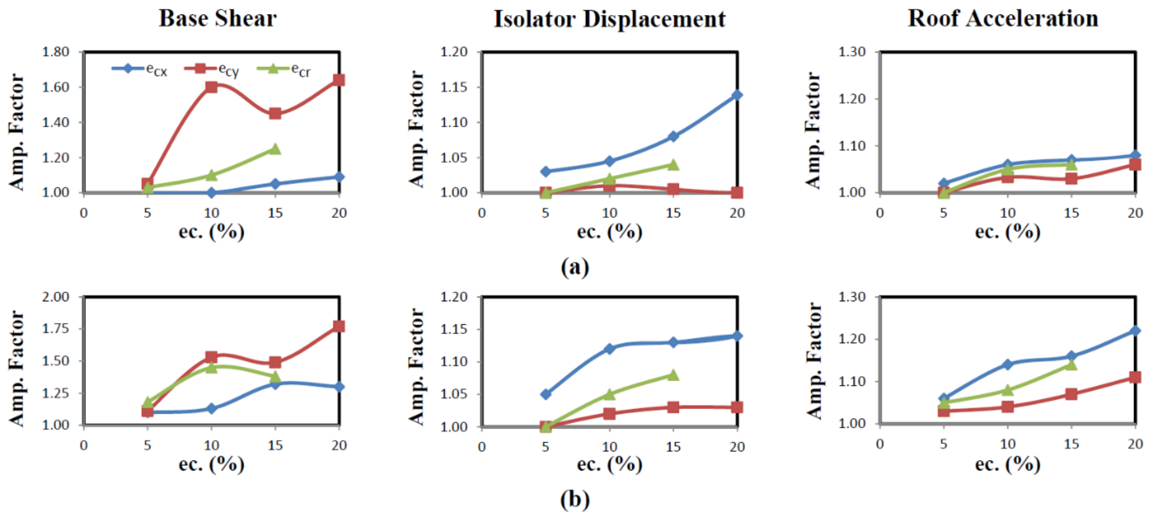

Fig. 11 Maximum Amp. Factor resulted from $E_{S\&B}$ in structure with β=1.33, γ=1 under simplified pulses having T_p=1-10s , PGV=40-200 cm/s (a) Fling step and (b) Forward directivity

Amp. Factors of different responses in isolation stiffness eccentricity case (E_B) are demonstrated in Fig. 10. As can be seen in this Fig., the Amp. Factors are significantly lower than the factors presented in Fig. 9 for E_S case. It can be concluded that the isolator stiffness eccentricity is less important comparing with mass eccentricity in superstructure. The result is in accordance with previous investigations (Khoshnoudian and Imani Azad 2011, Tena-Colunga and Zambrana-Rojas 2006). In the stiffness eccentricity (E_B) case, the maximum amplification of base shear is 1.28 in e_{cy}=20% of plan width. On the other hand, the isolator displacement and roof acceleration are intensified up to 1.06 and 1.11 respectively in e_{cx}=20% of plan length.

Fig. 11 displays the Amp. Factors where the mass and stiffness eccentricities simultaneously occur ($E_{S\&B}$). Comparison of the results of this Fig. with Fig. 9 reveals that coinciding of the center of mass with the center of stiffness decreases the torsional effects. For example, the maximum base shear Amp. Factor in Fig. 9 is 2.55 for e_{cy}=20% model under forward directivity pulses, while this factor is dropped to 1.77 in Fig. 11. Similarly the isolator displacement Amp. Factor is reduced from 1.30 in Fig. 9 to 1.14 in Fig. 11 under fling step pulses. Almazan and de la Llera (2003) have also revealed that the torsional amplification is declined when the center of mass coincides with the center of stiffness of SFP isolators in a 6-story base-isolated structure. Note that according to Kilar and Koren (2009) this reduction is more essential in the responses captured at the level of base isolation i.e., isolator displacement and base shear, but not in the superstructure level i.e., acceleration and drift of the stories. In addition, all the responses corresponding to forward directivity pulses are more than fling step ones.

Comparing the results of Figs. 9-11 obviously highlights two essential conclusions. Firstly, among all eccentricity cases the superstructure mass eccentricity is dramatically more significant than others. Thus, only the superstructure mass eccentricity will be considered in next chapters of current paper. Secondly, the base shear is affected by the eccentricity along the direction of input earthquake; whereas the eccentricity normal to the pulse direction affects the displacement and acceleration intensification due to torsion.

6.2 Mass eccentricity in different superstructures

It was confirmed that the mass eccentricity is more crucial in seismic responses of asymmetric isolated structures. In this section, the effect of mass eccentricity in different superstructures presented in Table 1 is investigated elaborately. For this purpose, all the models are analyzed under fling step and forward directivity pulses with T_p varies from 1s to 10s and PGV changes between 40 to 200 cm/s. The maximum Amp. Factor calculated by Eq. (6) is presented in this chapter. Note that only the results of e_{cx} eccentricity are illustrated.

The Amp. Factors of models with various slenderness ratios (β) are given in Fig. 12. It reveals that the 3-story structure with β=0.67 has the maximum base shear Amp. Factor. The factors are 1.77, 1.58 and 1.2 for structures assuming β equal to 0.67, 1.33 and 2 in the same order under forward directivity pulses. The structures with lower weight, the rocking motion due to earthquake pulses is more severe and makes significant changes in the distribution of vertical loads on the isolators. As discussed earlier the horizontal force of frictional bearings is dependents to their vertical weight; consequently, the amplification in the 3-story structure is importantly larger than 6-story or 9-story models. Note that in the results related to fling step pulses in this Fig. the 3-story structure with β=0.67 shows very small amplification factors.

The displacement Amp. Factor is similar for structures with different slenderness ratio. The maximum value is nearly 1.32 exhibited in structure with β=2 under fling step pulses. The 9-story model has experienced the greatest amounts of Amp. Factor for roof acceleration as 1.73 and 2.16 subjected to fling step and forward directivity pulses respectively. It is well justified as the total height of this structure is more than the others, the acceleration intensification is higher in the top floors.

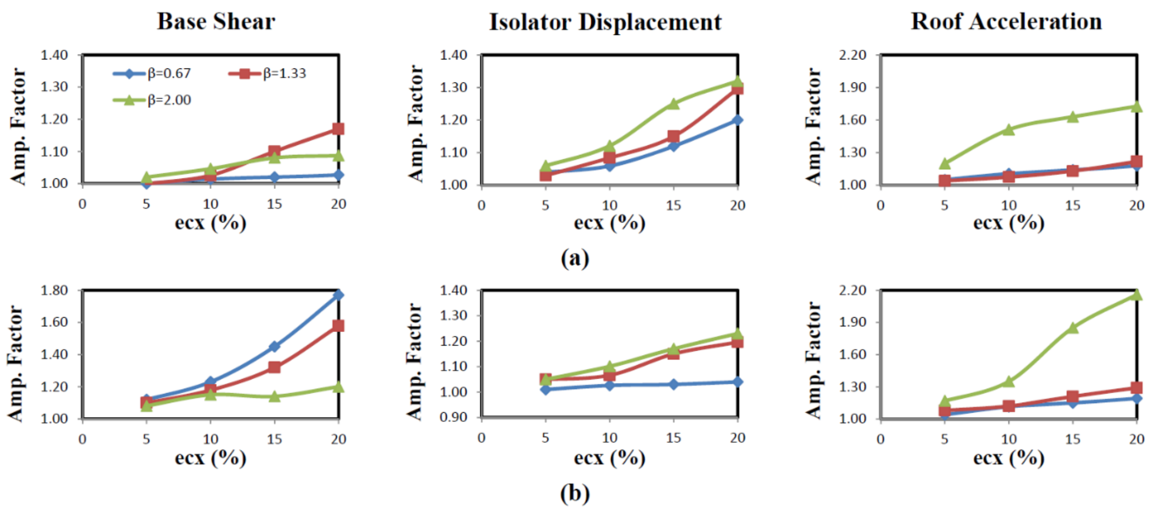

Fig. 12 Maximum Amp. Factor resulted from longtidunal E_S in structure with γ=1 and different slenderness ratio (β) under simplified pulses having T_p=1-10s, PGV=40-200 cm/s (a) Fling step and (b) Forward directivity

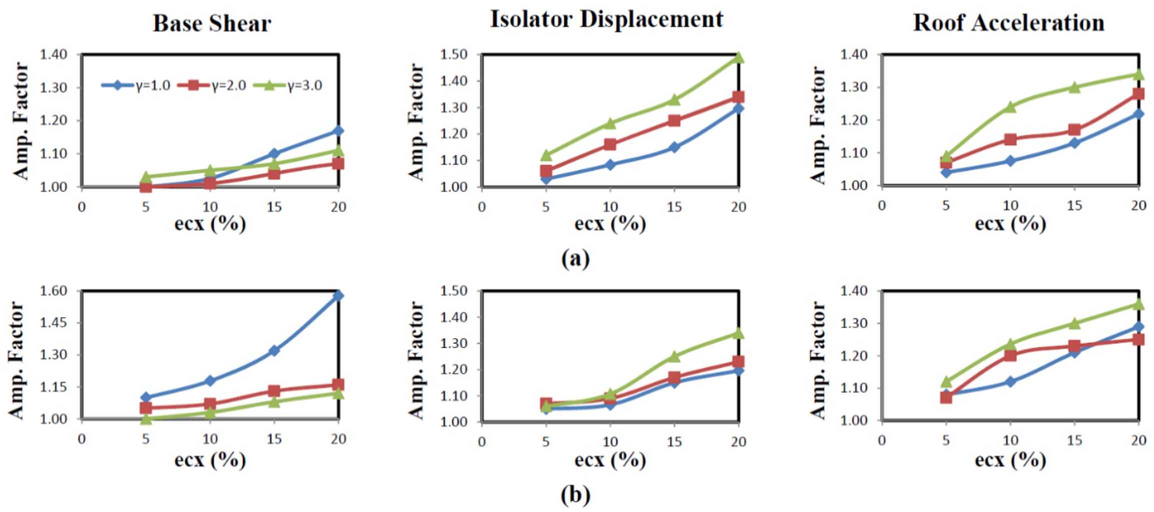

Fig. 13 Maximum Amp. Factor resulted from longtidunal E_S in structure with β=1.33 and different aspect ratio (γ) under simplified pulses having T_p=1-10s , PGV=40-200 cm/s (a) Fling step and (b) Forward directivity

It can be seen from the Fig. 13 that the aspect ratio (γ) hardly affects the Amp. Factor of different responses. Increasing this ratio from 1 to 3, the base shear amplification is reduced from 1.17 to 1.11 under fling step pulse and from 1.58 to 1.12 for forward directivity one. It was noted that structures with lower weight are more sensitive to base shear changes and the aspect ratio has negligible effect. Unlike the base shear, increase in γ raises the displacement and roof acceleration Amp. Factor because of larger distance between the center of mass and center of isolators in asymmetric rectangular plans. For example, the amplification factor in a structure with γ=1 is 1.20 and 1.29 for displacement and acceleration respectively, while they grow to 1.34 and 1.36 in the structure with γ=3 subjected to forward directivity pulses.

6.3 Drift changes due to mass eccentricity

The drift of base-isolated structure is hardly notable; thereby few investigations have been focused on it. In this research, some pulses with high velocity causes the isolator slider to hit the restrainer. Because of this pounding, the model temporarily behaves the same as a fixed-base structure. Admittedly, the interstory drift is increased in these pulses. In order to investigate the variations of drift, the peak drift of structures with 3, 6 and 9-story subjected to forward directivity pulses with T_p=1-4s and PGV=120 cm/s is illustrated in Fig. 14. It was demonstrated in section 5.2 that pulses with periods longer than 4s shows smaller responses.

Considering Fig. 14 results, the maximum drift of 3, 6 and 9-story symmetric structures are 0.05, 0.29 and 0.23% respectively for isolated structures under forward directivity pulse with T_p=4s. The mass eccentricity intensifies the interstory drift, for example, in 3, 6 and 9-story models, e_{cx}=20% raise the drift to 0.2, 0.65 and 0.73% respectively.

It is seen in Figs. 14(b) and 14(c) that the pattern of drift ratios of whole structure in e_{cx}=20% case is different from the other graphs of Fig. 14. This pattern is similar to a drift pattern of a structure with fixed columns in which the drift increases from lower stories to upper ones. It was noted that when isolated structures excited by pulses with great velocity, because of isolator pounding with its restrainer, the model transiently behaves like a structure without any base isolation. In the cases shown in Fig. 14, although there is no pounding between isolator and restrainer in symmetric models (e_{cx}=0), the mass eccentricity results this pounding. Therefore, it is concluded that mass eccentricity can expedite the pounding under some pulses with moderate PGV (e.g., 120 cm/s).

To better clarify the role of mass eccentricity on the amplification of interstory drift, a comparison is made between resultant drift and its allowable value in ASCE 7-10 standard. According to this code, the maximum allowable plastic drift that is calculated according to Eq. (7) in a base-isolated structure is 1.5%.

$$\delta_p = \frac{R\delta_e}{I_e} < 1.5\% \tag{7}$$

Where δ_p and δ_e are plastic and elastic drifts respectively, R stands for structure response factor that is equal to 2 and I_e denotes importance factor which is assumed 1 according to ASCE recommendation for isolated structures (ASCE 7, 2010). Based on the Eq. (7) the allowable elastic drift is equal to 0.75% which is drawn as a limit on graphs of Fig. 14. It is important to note that, whereas the superstructure is linearly modeled in this research, the elastic drift is considered as allowable limit. It is clear from Fig. 14(c), that the eccentricity makes the drift ratio to nearly reach the allowable value in 6-story structure.

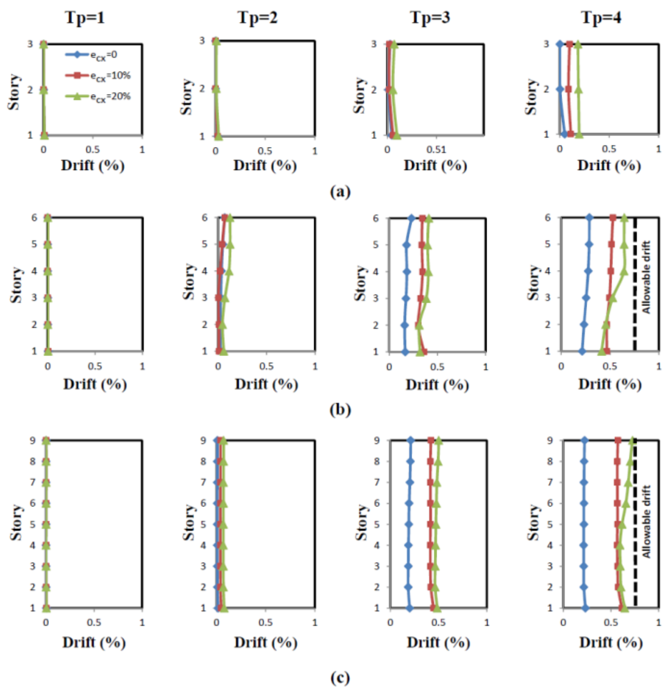

Fig. 14 Maximum Drift in structures with longtidunal E_S under forward directivity pulses assuming γ=1, T_p=1-4s, PGV=120cm/s (a) β=0.67, (b) =1.33 and (c) =2.00

7. Isolator properties

A TCFP isolator with T_{eff}=5s and ξ_{eff} =15% was used in chapters 5 and 6. In order to generalize the conclusions for isolators with different properties, several isolators are designed according to Eqs. (4) and (5) which are presented in Table 2. The displacement capacity of all isolators is assumed 1m. A symmetric superstructure with β=1.33 and γ=1 is mounted on the isolators reported in Table 2 and the models are subjected to fling step and forward directivity pulses with T_p=1s-10s and PGV=40-200 cm/s. As an example, the results for isolators with different effective period and damping ratio under forward directivity pulse with T_p=1s is presented in Fig. 15. It is noted that similar trends are obtained from other studied cases.

Table 2 Properties of different TCFP isolators

Design	T_{eff}	ξ_{eff}	Displacement Capacity-D (m)			Effective Radii-R_{eff} (m)		Friction Coefficient-μ		
	(sec)	(%)	d_1=d_4	d_2=d_3	D(Total)	R_{eff1}= R_{eff4}	R_{eff2}= R_{eff3}	μ_2= μ_3	μ_1	μ_4
TCFP-1	3	15	0.45	0.05	1.0	2.0	0.3	0.05	0.115	0.2
TCFP-2	4	15	0.45	0.05	1.0	3.5	0.3	0.02	0.06	0.11
TCFP-3	5	15	0.45	0.05	1.0	5.5	0.45	0.02	0.04	0.07
TCFP-4	5	10	0.45	0.05	1.0	5.5	0.45	0.02	0.025	0.06
TCFP-5	5	20	0.45	0.05	1.0	5.5	0.45	0.02	0.06	0.07
TCFP-6	5	30	0.45	0.05	1.0	7.0	0.45	0.02	0.09	0.10

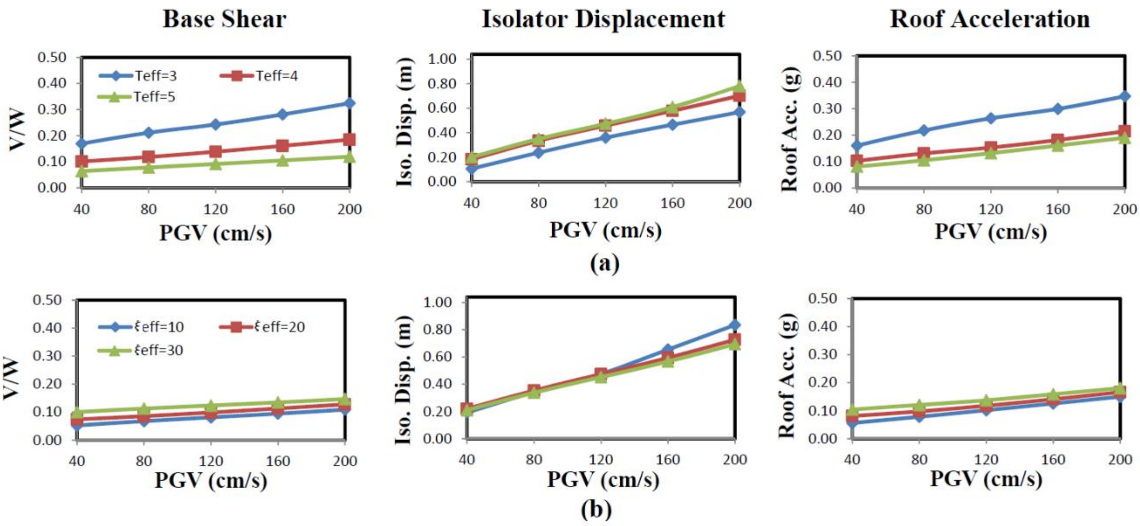

Fig. 15 Responses of structures with β=1.33, γ=1 under forward directivitypulse assuming T_p=1s (a) Isolators with different periods and (b) Isolators with different damping

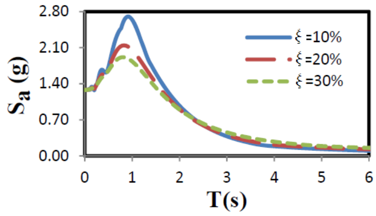

Fig. 16 Acceleration spectra of forward directivity pulse with T_p=1s, PGV=200 cm/s

The isolators with lower damping has greater displacement (Fig 15(b)); i.e., increasing the damping ratio from 10 to 30 percent decreases the displacement in PGV=200 cm/s from 83 to 69 cm. The role of damping in changing the base shears as well as roof accelerations is negligible. Fig. 16 can clearly reveal why the isolator damping effect is significantly less than its period in changing different responses. In this Fig. the acceleration spectra of forward directivity pulse assuming T_p=1s and PGV=200 cm/s with damping ranges from 10-30 percent are drawn. It can be concluded that in high period ranges, specifically periods more than 3s, the damping has minimum effect on the input acceleration of structure and therefore on the responses.

8. Conclusions

This investigation is carried out to demonstrate the effects of mathematical near-fault pulse models on the responses of asymmetric structures isolated with the TCFP. The effects of longitudinal, transversal and diagonal mass and stiffness eccentricities in intensifying the responses of isolated structures, namely base shear, displacement, acceleration and drift are emphasized as well. A reasonable variety of superstructures with different aspect ratios i.e., 1, 2 and 3 and slenderness ratios of 0.67, 1.33 and 2 as well as TCFP isolators with different effective damping and period are considered. The TCFP effective period and damping varies from 3 to 5 seconds and 10 to 30% in the same order. The linear three-dimensional model is assumed for superstructure while the isolators are nonlinearly simulated. The results of this study can be summarized as follows:

- The superstructure mass eccentricity causes the most torsional effects comparing with other eccentricity cases on base-isolated structure mounted on TCFP bearings. Simultaneous occurrence of mass and stiffness eccentricities decrease the effects of mass eccentricity. In a 6-story structure, the base shear and displacement amplification factors are 2.55 and 1.30 considering mass eccentricity, while they are fallen to 1.77 and 1.14 respectively in simultaneous eccentricity of mass and stiffness. The stiffness eccentricity of isolators has minimum effect on the amplification of various responses.
- The responses of isolated structures subjected to forward directivity pulses are mostly greater than the fling step ones. In 6-story structure, the longitudinal mass eccentricity intensifies the isolator displacement as 30 and 20 percent under fling step and forward directivity pulses respectively. This growth is similarly 73 and 116 percent for acceleration of 9-story model; furthermore, 17 and 77 percent in the base shear of 3-story structure.

- Increasing the aspect ratio in plan from 1 to 3, rises the displacement amplification factor due to torsion from 1.20 to 1.34 as well as acceleration amplification factor from 1.29 to 1.36 under forward directivity pulses.
- In the both fling step and forward directivity pulses, the increase of PGV raises the responses. In a forward directivity pulse with T_p=2s and PGV=40 cm/s the base shear, displacement and acceleration of a 6-story model is 0.08W, 0.33m and 0.09g in the same order. In a similar pulse with PGV=200 cm/s the results grows to 0.59W, 1m and 1.43g respectively. It shows the key factor of PGV on the studied research.
- It can be concluded that in the both investigated pulses, increasing the T_p from 1s to 4s raises all the responses. However, the responses decrease when the T_p rises from 4s to 10s. It means that when T_p/T_{eff} tends to 1, the structural responses increase significantly.
- In some high velocity near-fault pulses, because of pounding between isolator slider and restrainer, the model temporarily behaves like a fixed-base structure. As a result, the interstory drift is increased significantly. The maximum drift of asymmetric 9-story structure under forward directivity pulses is nearly 0.73%. Note that the allowable elastic drift is equal to 0.75% according to ASCE 7. Therefore, the eccentricity causes to reach the allowable limit of drift ratio.

References

Agrawal, A.K. and He, W.L. (2002), "A closed-form approximation of near-fault ground motion pulses for flexible structures", *Proceedings of the 15th ASCE engineering mechanics conference*, Columbia University, New York, NY.

AISC (2010), "Seismic Provisions for Structural Steel Buildings", ANSI/AISC 341-10, American Institute of Steel Construction, Chicago, Illinois, USA.

AISC (2010), "Specification for Structural Steel Buildings", ANSI/AISC 360-10, American Institute of Steel Construction, Chicago, Illinois, USA.

Akkar, S., Yazgan, U. and Gulkan, P. (2005), "Drift estimates in frame buildings subjected to near-fault ground motions", *J. Struct. Eng. -ASCE*, **131**(7), 1014-1024.

Alavi, B. and Krawinkler, H. (2004), "Behavior of moment-resisting frame structures subjected to near-Field ground motions", *Earthq. Eng. Struct. D.*, **33**, 687-706.

Almazan, J.L. and De la Dlera, J.C. (2003), "Accidental torsion due to overturning in nominally symmetric structures isolated with the FPS", *Earthq. Eng. Struct. D.*, **32**, 919-948.

ASCE 7-10 (2010), "Minimum Design Loads for Building and Other Structures", ASCE/SEI 7-10, American Society of Civil Engineers, Reston, Virginia, USA.

Bagheri, M. and Khoshnoudian, F. (2014), "The effect of impact with adjacent structure on seismic behavior of base-isolated buildings with DCFP bearings", *Struct. Eng. Mech.*, **51**(2), 277-297.

Baker, J.W. (2007), "Quantitative classification of near-fault ground motions using wavelet analysis", *Bull. Seismol. Soc. Am.*, **97**(5), 1486-1501.

Becker, T.C. and Mahin, S.A. (2012), "Experimental and analytical study of the bi-directional behavior of the triple friction pendulum isolator", *Earthq. Eng. Struct. D.*, **41**, 355-373.

Becker, T.C. and Mahin, S.A. (2013), "Approximating peak responses in seismically isolated buildings using generalized modal analysis", *Earthq. Eng. Struct. D.*, **42**, 1807-1825.

Bertero, V., Mahin, S. and Herrera, R. (1978), "Aseismic design implications of near-fault San Fernando earthquake records", *Earthq. Eng. Struct. D.*, **6**(1), 31-42.

Dao, N.D., Ryan, K.L., Sao, E. and Sasaki, T. (2013), "Predicting the displacement of triple pendulum bearings in a full-scale shaking experiment using a three-dimensional element", *Earthq. Eng. Struct. D.*,

42, 1677-1695.
De la Llera JC, Almazan JL. (2003) “An Experimental Study of Nominally Symmetric and Asymmetric Structures Isolated with the FPS”, Earthquake Engineering and Structural Dynamics **32**: 891-918.
De la Llera, J.C. and Chopra, A.K. (1994), “Accidental torsion in buildings due to base rotational excitation”, *Earthq. Eng. Struct. D.*, **23**, 1003-1021.
Dicleli, M. (2007), “Supplemental elastic stiffness to reduce isolator displacements for seismic-isolated bridges in near-fault zones”, *Eng. Struct.*, **29**, 763-775.
Dicleli, M. and Buddaram, S. (2007), “Equivalent linear analysis of seismic-isolated bridges subjected to near-fault ground motions with forward rupture directivity effect”, *Eng. Struct.*, **29**, 21-32.
Fallahian, M., Khosnoudian, F. and Loghman, V. (2015), “Torsionally seismic behavior of triple concave friction pendulum bearing ”, *Adv. Struct. Eng.*, Accepted in Press.
Fenz, D. and Constantinou, M.C. (2008a), “Mechanical behavior of multi-spherical sliding bearings”, Technical Report No. MCEER-08/0007, State University of New York at Buffalo, Buffalo. New York, USA.
Fenz, D. and Constantinou, M.C. (2008b), “Modeling triple friction pendulum bearings for response history analysis”, *Earthq. Spectra*, **24**, 1011-1028.
Galal, K. and Naemi, M. (2008), “Effect of soil conditions on the response of reinforced concrete tall structures to near-fault earthquakes”, *Struct. Des. Tall Spec.*, **17**, 541-562.
Ghahari, S.F. and Khaloo, A.R. (2013), “Considering rupture directivity effects, which structures should be named ‘Long-Period Buildings’?”, *Struct. Des. Tall Spec.*, **22**, 165-178.
Hall, J.F., Heaton, T.H., Halling, M.W. and Wald, D.J. (1995), “Near-source ground motion and its effects on flexible buildings”, *Earthq. Spectra*, **11**(4), 569-605.
Jangid, R.S. (2005), “Optimum friction pendulum system for near-fault motions”, *Eng. Struct.*, **27**, 349-359.
Jangid, R.S. and Datta, T.K. (1995), “Performance of base isolation systems for asymmetric building subjected to random excitation”, *Eng. Struct.*, **17**(6), 443-454.
Jangid, R.S. and Kelly, J.M. (2001), “Base isolation for near-fault motions”, *Earthq. Eng. Struct. D.*, **30**, 691-707.
Kalkan, E. and Kunnath, S.K. (2006), “Effects of fling step and forward directivity on seismic response of buildings”, *Earthq. Spectra*, **22**, 367-390.
Khoshnoudian, F. and Ahmadi, E. (2013), “Effects of pulse period of near-field ground motions on the seismic demands of soil–MDOF structure systems using mathematical pulse models”, *Earthq. Eng. Struct. D.*, **42**(11), 1565-1582.
Khoshnoudian, F. and Azizi, N. (2007), “Nonlinear response of a torsionally coupled base-isolated structure”, Proceedings of the ICE - Structures and Buildings, **160**, 207-219.
Khoshnoudian, F. and Imani Azad, A. (2011), “Effect of two horizontal components of earthquake on nonlinear response of torsionally coupled base isolated structures”, *Struct. Des. Tall Spec.*, **20**, 986-1018.
Khoshnoudian, F. and Motamedi, D. (2013), “Seismic response of asymmetric steel isolated structures considering vertical component of earthquakes”, *J. Civil Eng. - KSCE*, **17**(6), 1333-1347.
Khoshnoudian, F. and Rabiei, M. (2010), “Seismic response of double concave friction pendulum base-isolated structures considering vertical component of earthquake”, *Adv. Struct. Eng.*, **13**(1), 1-13.
Khoshnoudian, F. and Rezai Haghdoost, V. (2009), “Responses of pure-friction sliding structures to three components of earthquake excitation considering variations in the coefficient of friction”, Scientia Iranica, Transaction A: Civil Engineering, **16**(6), 429-442.
Kilar, V. and Koren, D. (2009), “Seismic behaviour of asymmetric base isolated structures with various distributions of isolators”, *Eng. Struct.*, **31**, 910-921.
Krawinkler, H. and Alavi, B. (1998), “Development of an improved design procedure for near-fault ground motions”, SMIP 98 seminar on utilization of strong motion data, Oakland, CA.
Loghman, V. and Khoshnoudian, F. (2015), “Comparison of seismic behavior of long period SDOF systems mounted on friction isolators under near-field earthquakes”, *Smart Struct. Syst.*, Accepted in Press.
Masaeli, H., Khoshnoudian, F. and Hadikhan Tehrani, M. (2014), “Rocking isolation of nonductile moderately tall buildings subjected to bidirectional near-fault ground motions”, *Eng. Struct.*, **80**, 298-315.

Morgan, T. and Mahin, S.A. (2010), "Achieving reliable seismic performance enhancement using multi-stage friction pendulum isolators", *Earthq. Eng. Struct. D.*, **39**, 1443-1461.

Morgan, T.A. and Mahin, S.A. (2011), "The Use of Base Isolation Systems to Achieve Complex Seismic Performance Objectives", Report No. PEER-2011/06, Pacific Earthquake Engineering Research Center (PEER), Berkeley, CA, USA.

Panchal, V.R. and Jangid, R.S. (2008), "Variable friction pendulum system for near-fault ground motions", *Struct. Control Health Monit*., **15**, 568-584.

Picazo, Y., Lopez, O.D. and Esteva, L. (2015), "Seismic reliability analysis of buildings with torsional eccentricities", *Earthq. Eng. Struct. D.*, **44**, 1219-1234.

Rabiei, M. and Khoshnoudian, F. (2011), "Response of multi-story friction pendulum base-isolated buildings including the vertical component of earthquake", *Canadian J. Civil Eng*., **38**, 1045-1059.

Rabiei, M. and Khoshnoudian, F. (2013), "Seismic response of elevated liquid storage tanks using double concave friction pendulum bearings with tri-linear behavior", *Adv. Struct. Eng*., **16**(2), 315-338.

Ryan, K.L. and Chopra, A.K. (2006), "Estimating bearing response in symmetric and asymmetric-plan isolated buildings with rocking and torsion", *Earthq. Eng. Struct. D*., **35**, 1009-1036.

Sarlis, A.A. and Constantinou, M.C. (2013), "Model of Triple Friction Pendulum Bearing for General Geometric and Frictional Parameters and for Uplift Conditions" Report No. MCEER-13-0010, State University of New York at Buffalo, Buffalo. New York, USA.

Sasani, M. and Bertero, V. (2000), "Importance of severe pulse-type ground motion in performance-based engineering: Historical and critical review", *Proceedings of the 12th world conference on earthquake engineering*, New Zealand, Paper No.8.

Siringurino, D.M. and Fujino, Y. (2015), "Seismic response analyses of an asymmetric base-isolated building during the 2011 Great East Japan (Tohoku) earthquake", *Struct. Control Health Monit*., **22**, 71-90.

Tajammolian, H., Khoshnoudian, F. and Partovi Mehr, N. (2016), "Seismic responses of isolated structures with mass asymmetry mounted on TCFP subjected to near-fault ground motions", *Int. J. Civil Eng*., DOI 10.1007/s40999-016-0047-9.

Tajammolian, H., Khoshnoudian, F., Talaei, S. and Loghman, V. (2014), "The effects of peak ground velocity of near-field ground motions on the seismic responses of base-isolated structures mounted on friction bearings", *Earthq. Struct*., **7**(6), 1259-1282.

Tena-Colunga, A. and Escamilla-Cruz, J. (2007), "Torsional amplifications in asymmetric base isolated structures", *Eng. Struct*., **29**(2), 237-247.

Tena-Colunga, A. and Gomez-Soberon, L. (2002), "Torsional response of base isolated structures due to asymmetries in the superstructure", *Eng. Struct*., **24**, 1587–1599.

Tena-Colunga, A. and Zambrana-Rojas, C. (2006), "Dynamic torsion amplifications in asymmetric base isolated structures with an eccentric isolation system", *Eng. Struct*., **28**(3), 72-83.

Zayas, V.A., Low, S.S. and Mahin, S.A. (1987), "The SFP Earthquake Resisting System: Experimental Report", Report No. UCB/EERC-87/01, Earthquake Engineering Research Center, University of California Berkeley, Berkeley, CA, USA.

Zayas, V.A., Low, S.S., Bozzo, L. and Mahin, S.A. (1989), "Feasibility and Performance Studies on Improving the Earthquake Resistance of New and Existing Buildings Using the Friction Pendulum System", Report No. UCB/EERC-89/09, Earthquake Engineering Research Center, University of California Berkeley, Berkeley, CA, USA.

Zhang, J. and Tang, Y. (2009), "Dimensional analysis of structures with translating and rocking foundations under near-fault ground motions", *Soil Dyn. Earthq. Eng*., **29**, 1330-1346.

CC